¹Houshyar Keyhanifar

1*Jamasb Pirkandi

¹Reza Zardashti,

¹Keramat Malekzadehfard

Identification of Autonomous Air Refueling Using Parametric Sigmoid Neural Networks Considering Turbulence Effects



Abstract: - In this research, the problem of improving probe and drogue identification in aerial refueling systems in the presence of uncertainty is investigated. This uncertainty is caused by the effects of environmental turbulence and tanker aircraft turbulence on the aerodynamic parameters of the refueling aircraft. The purpose of this work is to identify aerial refueling aircraft and extract control parameters for the development of the automatic aerial refueling system of tanker aircraft. To do this, a non-linear model of receiver airflow is developed, taking into account tanker airflow and environmental turbulence effects. In the second step, the desired algorithm is designed by combining a nonlinear neural network with a parametric sigmoid function. Automation of such a scenario requires many activities to be performed by algorithms that are delegated to trained crews. After mathematical modeling and obtaining the input and output values with MATLAB software, learning algorithms have been used to train them with the network. In this case, after each repetition, the average error of the network in the output production is reduced to achieve convergence. The training error is usually reduced in the initial stage of the training connection. By comparing the results, it can be seen that the proposed method has a better performance than conventional methods in reducing the mode errors between two planes and limits all signals uniformly.

Keywords: aerial refueling, Identification, Parametric Sigmoid, Neural network, Turbulence effects, Probe and Drogue

I.INTRODUCTION

The use of automatic aerial refueling (AAR) has reduced the number of personnel per aircraft (A/C) while reducing the risk of human crews, which can increase the accuracy and speed of operations and avoid additional long-term support costs. The purpose of AAR is to increase the flight duration, increase the carrying capacity of combat equipment and commercial cargo, reduce the cost of the flight fleet and increase the life of A/C [1-4].

In AAR, there are two different refueling mechanisms [5]: aerial refueling (AR) by boom and receptacle (BAR) and by probe and drogue (PAD) mechanisms, and both of them are important in applications. PAD systems are more flexible and simpler than BAR systems.

This research investigated AR using the PAD method [6]. This refueling method can be used at various refueling speeds and refuel several receiver A/Cs simultaneously. In the PAD method, the receiver A/C follows the flexible hose and drogue at the end of the hose. The hose is pulled on the back and bottom of the tanker A/C. The drogue nose is closed at the end of the hose and the probe is mounted on the receiver A/C.

During the AR process, the receiver A/C approaches a predetermined route from the bottom and behind the tanker A/C. The tanker A/C flies in a level and straight direction with a uniform linear motion at a constant speed and altitude. The present study attempts to use convolutional neural networks (CNN) as a subset of artificial neural networks (ANN) to identify visual A/C. A robust positioning method is crucial to the achievement of the goals of an autonomous A/C guided by artificial intelligence. Position understanding, in turn, requires accurate and automatic recognition to convert information into data. So, a firm understanding of the environment helps maintain the A/C. Therefore, proper machine intelligence, to control an A/C independently requires much more than improved pattern recognition. This study applies recent academic advances in identifying visual patterns with ANN to improve the understanding of refueling A/C. A tanker A/C, equipped with a machine vision (MV) system, can align the rear cameras with a standard approach vector. This makes the A/C view close to the refueling approach as seen from the front and above. Images of the AAR are placed into a system that creates the type of A/C for any video frame used to direct the performance of other autonomous systems in the AR process [7].

Copyright © JES 2024 on-line: journal.esrgroups.org

¹ Faculty of Aerospace, MalekAshtar University of Technology, Tehran, Iran.

^{*} Corresponding author

Using sensors based on Global Positioning System (GPS), MV, laser, and infrared radar has many applications. Nevertheless, there are always operational restrictions. The GPS signals may not have adequate coverage in different parts of the world. In addition, it may not always be possible to use the GPS signals of the receiver A/C [8]. The MV sensors are widely used in AAR. Relative position and rotation can be achieved using these sensors by detecting and identifying target-marked data and two-dimensional camera images. The MV sensor's accuracy is high and can cover different frequencies. However, the use of an MV sensor is limited due to the distance between the sensor and the target [9].

Due to the extensive research on automatic refueling systems, several activities have been reviewed below. In a study, Campa et al. [10] examined the MV development for AR. They found an MV algorithm to calculate the position and rotation between the Unmanned Aerial Vehicle (UAV) and the tanker A/C. They used a simple linear interpolation method to combine the sensors in AR. However, the linear interpolation method could not contain information about the sensor malfunction characteristics due to its simplification. Philip et al. [11] in a study examined the status and control estimation for the docking phase. They used different estimators for position parameters based on MV output. They also obtained a fixed-interest observer to estimate the position and condition of the two A/C. Sinopli et al. [12] examined the A/C performance when approaching each other based on the GPS/Inertial Navigation system (INS). In this research, based on the UAV model, they planned a route from the initial state to the final state, and then, by moving the UAV in the defined path, they obtained more information from the camera to aid in the identification. In a study, Borui et al. [13] investigated the AR issue using the multi-sensor combination method. In this study, they showed that MV technology is an effective method for achieving the accuracy required between two A/Cs. They also proved that using filters is a useful way to combine multiple sensors.

L.R. Mash [14] concluded in a study that a neural network is adequately and appropriately trained in much the same way that the flight crew learns to identify the A/C. It requires three consecutive and relevant research areas: optimized parameter selection, optimal data reinforcement, and combination and collection. There are many questions about how to design and train a network for a specific classification range. The first sub-question of the research is: What set of network design parameters describes the A/C, shape, network capacity, and performance optimization of object classification in a specific diagnosis area? He assumed that the general machine learning principle, which is deep learning, can be used to achieve optimal network configuration. An increasing amount of data is used to improve the neural network's ability to generalize usefully to a wider range of possible inputs for training data in deep learning. The second sub-question to be considered is: What combination of data enhancement techniques is more applicable to the specific task of A/C classification? A positive function is assumed when rotation, obstruction, and scaling are applied randomly. However, these computational techniques are complex. Therefore, performance improvement should be considered against the deterrent calculations' complexity. Mesh et al. [15] showed that a set of trained NNs exhibits better performance than individual networks .The sum structure of groups naturally provides a reliable amount that is associated with the output accuracy of the sets. It was also examined that the set of assurances is useful for implementing a decision-making framework. Using the combination of MV and GPS, Keyhanifar et al. [16] identified and controlled the receiver A/C in the presence of the vortex created by the tanker A/C and atmospheric turbulence. It was also used to integrate information to obtain a relative position between the receiver A/C and drogue. The simulation results with MATLAB software indicated a safe and successful connection between the two A/Cs. However, the proposed approach in this article requires approval and practical validation by conducting refueling flight tests that have not been carried out. In the field of deep learning, increasing data is a strategy used to improve NN's generalization capabilities over a wider range of possible inputs than training data alone. Kanazawa et al. [17], showed that each educational image shows the sample of a particular location in a high-dimensional impact function that is learned by a NN during training. Krogh et al. [18] used the composition of trained NNs and proved that the combination of NNs was significantly better. Moreover, in identifying the receiver A/C, the combined structure provides a reliable amount that correlates with output accuracy.

But there is a problem and that is manned air-to-air refueling is a difficult task for the pilot, especially in bad weather conditions. Therefore, AAR is considered a challenging task and without the presence of a skilled pilot in the cockpit, it becomes a control system challenge during AR maneuver. For AAR to be successful, the receiver

A/C must maintain its precise position relative to the tanker A/C, and this is only possible by developing the appropriate control system. The research aims to develop an identification system for safe guidance of the A/C.

Despite the analyses performed by the researchers, there are still challenges in designing the docking identification of the A/C aerial refueling because there are precise and sensitive requirements such as tracking error and the relative speed limit between the two A/Cs for PAD. In this research, an NN with parametric sigmoid function (PSF) based on a Fusion Sensor (FS) strategy using MV data and DGPS is applied to the receiver A/C identification. In addition, using NN-PSF, the problem of identifying AAR with high precision even when there are effects such as downwash, turbulences, and uncertainty is also solved. The proposed NN-PSF method, when considering additional parameters in the activation functions of NN and changing their shapes by adjusting the parameters, will increase the network flexibility.

The main contributions of this work are listed as follows:

- 1. A new framework for PAD-Receiver (UAV) connectivity based on a FS strategy using MV and DGPS data has been proposed.
- 2- Using neural networks with PSF, results such as: A. Favorable accuracy and high learning speed; B. Sensitizing the network and Preventing reduction of the excessive absolute function value due to the of natural logarithms utilization in the transfer functions, and; C. Reducing the error between the receiver and tanker.

Description of the PAD system

Figure 1 shows the PAD system, having a flexible hose mounted below and behind the tanker A/C. At the end of this hose is a conical drogue. The probe is then placed on the receiver A/C. In this process, the receiver A/C sends the probe into the drogue, where it locks in place and refueling begins. The receiver A/C waits to receive in-flight fuel.

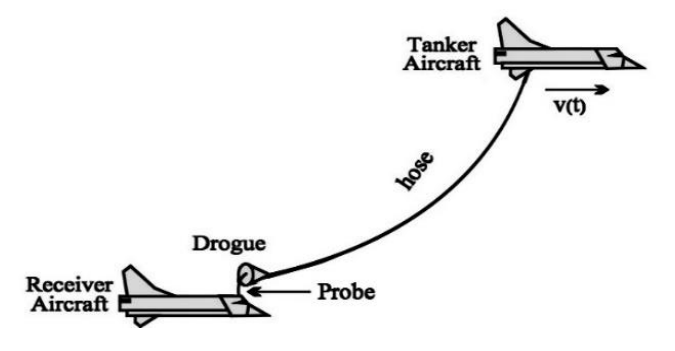


Fig. 1. PAD aerial refueling system

Reference coordinates and measuring sensors

To study the AR problem, it is necessary to introduce and recognize coordinate reference devices, distance measuring sensors, and distance vectors between A/C, drogue, and camera.

Reference coordinate system

Figure 2 is to introduce a reference frame in the AR system. In this figure, OERF is the reference frame located on the ground, OTRF is the reference frame located on the tanker A/C, ORRF is the reference frame mounted on the receiver A/C, OCRF is the reference frame mounted on the camera and ODRF is the reference device mounted on the drogue [19].

Distance measurement sensors

Both refueling A/Cs are assumed to be equipped with DGPS and radio communication. It is also assumed that DGPS makes measurements on ORRF and OTRF frames and that the receiver A/C is equipped with an MV to restore relative position during the connection process. MV receives images of designated points on the tanker A/C. MV images are provided on the x, and z planes on the OCRF to facilitate display [19].

The distance vectors

The distance vectors in AAR are shown in Figure 2 as follows.

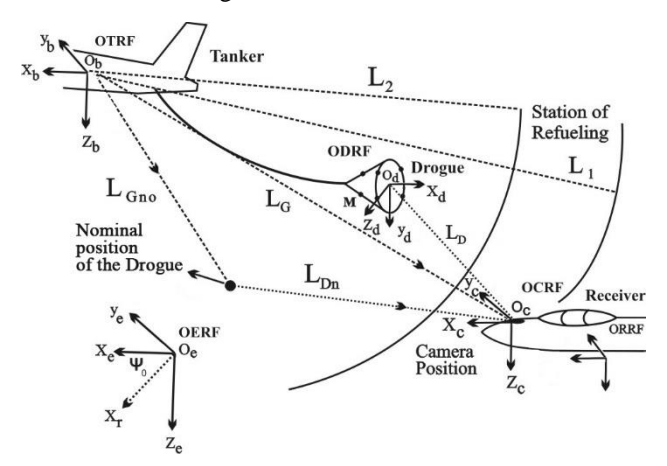


Fig.2.AAR reference coordinate and distance vectors

DGPS - related distance

A receiver A/C with a DGPS sensor can calculate the relative distance between two A/Cs. The camera is mounted on the receiver A/C and measures the L_G distance.

Drogue actual distance

As shown in Figure 2, the vector L_{Gn0} represent the nominal position of the drogue and tanker A/C. The desired position in the receiving A/C reference frame is measured using the L_{Dn} vector.

$$L_{Dn} = L_G - L_{Gno}. (1)$$

Where L_G the distance between the two A/C, L_{Dn} the distance between the drogue and receiver A/C, L_{Gno} is the distance between the drogue and tanker A/C.

Distance of drogue based on MV

The L_D vector is the distance between the camera and drogue based on a MV sensor.

II.MODELING

A/C receiver model

A nonlinear model of receiver A/C is given in the reference [20]. In this paper, the KC-135 has been selected for tanker A/C and F-16 A/C due to its UAV-like model, selected for being the receiver A/C. The state vectors (*X*) for each A/C are selected as follows:

$$\mathbf{X} = [V, \alpha, \beta, P, q, r, \phi, \theta, \Psi, x, y, z]^{T}$$
(2)

Where V is the A/C velocity. β and α are the sideslip angles and angle of attack (AOA), respectively and P, q, r are the rotational velocities in the body reference frame, ϕ , θ , Ψ are Euler angles in the body reference frame and x, y, and z represent the translational positions in the ground reference frame. The control variables are selected as follows:

$$U = [\delta_a, \delta_e, \delta_r, \delta_t]^T \tag{3}$$

Where δ_a is aileron surface deflection, δ_e is elevator surface deflection, δ_r is rudder surface deflection and δ_t is throttle control variable. The assumptions for extracting the equations of receiver A/C are the rigid body, the constant mass, the rotation of the ground is ignored, the ignorance gravitational changes due to altitude and the C.G does not change the \bar{c} percentage. The equation of velocities and acceleration are extracted as follows:

• Translational velocities: for clarity, sin is abbreviated as s, cos as c and tan as t.

$$\dot{x}_R = V \left[c \alpha . c \beta . c \theta . c \psi + s \beta (s \theta . s \phi . c \psi - c \phi . s \psi) + s \alpha . c \beta (s \phi . s \psi + s \theta . c \phi . c \psi) \right]. \tag{4}$$

$$\dot{y}_R = V \left[c \beta. c \alpha. c \theta. s \psi + s \beta (s \phi. s \theta. s \psi + c \phi. c \psi) + c \beta. s \alpha (c \phi. s \theta. s \psi + s \phi. c \psi) \right]. \tag{5}$$

$$\dot{z}_R = V[-c\alpha.c\beta.s\theta + s\beta.c\theta.s\phi + s\alpha.c\beta.c\theta.c\phi]. \quad (6)$$

Where \dot{x}_R , \dot{y}_R , \dot{z}_R are translational velocities.

Acceleration relative to the ground and flow angles

$$\dot{V}_{k} = g(s\beta.s\phi.c\theta + c\beta.s\alpha.c\phi.c\theta - c\alpha.c\beta.s\theta) + \frac{1}{m}(-D + Tc\alpha.c\beta). \tag{7}$$

$$\dot{\beta}_{k} = p \cdot s \alpha - r \cdot c \alpha + \frac{g}{V} (c \alpha \cdot s \beta \cdot s \theta + c \beta \cdot s \phi \cdot c \theta - s \alpha \cdot s \beta \cdot c \phi \cdot c \theta) + \frac{1}{mV} (-S - T \cdot c \alpha \cdot s \beta). \tag{8}$$

$$\dot{\alpha}_{k} = q - r.s\alpha.t\beta - pc\alpha.t\beta + \frac{g}{c\beta V} \left[(s\alpha.s\theta + c\alpha.c\phi.c\theta) + \frac{1}{mV} (-L - T.s\alpha) \right]. \tag{9}$$

• Angular velocities

$$\dot{\phi} = p + q\sin\phi\tan\theta + r\cos\phi\tan\theta. \tag{10}$$

$$\dot{\theta} = q\cos\phi - r\sin\phi. \tag{11}$$

$$\dot{\psi} = (q\sin\phi + r\cos\phi)\sec\theta \ . \tag{12}$$

Where $\dot{\phi}$, $\dot{\theta}$, $\dot{\psi}$ are angular velocities.

Rotational velocities

$$\dot{p} = \frac{1}{I_x I_z - I_{xz}^2} \left[\left(I_y I_z - I_z^2 - I_{xz}^2 \right) rq + \left(I_x I_{xz} - I_y I_{xz} - I_z I_{xz} \right) pq + I_z \mathcal{L} + I_{xz} N. \right]$$
(13)

$$\dot{q} = \frac{1}{I_v} [(I_z - I_x)pr - I_{xz}p^2 + I_{xz}r^2 + M]. \tag{14}$$

$$\dot{\mathbf{r}} = \frac{1}{I_x I_z - I_{xz}^2} \left[\left(I_x^2 - I_x I_y + I_{xz}^2 \right) pq - \left(I_x I_{xz} - I_y I_{xz} - I_z I_{xz} \right) rq + I_{xz} \mathcal{L} + I_x N \right]. \tag{15}$$

Where \dot{p} , \dot{q} , \dot{r} are **rotational velocities and** I_x , I_y , I_z are momentum of inertia in the direction X, Y, Z and \mathcal{L} , M, N are moments along the axis.

PAD system model

The PAD system is modeled as a link-connected system, where the hose consists of a limited number of rigid cylindrical connections connected to spherical connections without friction. The masses and loads associated with each joint are concentrated in the joints. Drogue acts as a lumped mass at the end of the tanker A/C hose. It is modeled based on the finite element model and uses a limited number of rigid cylindrical joints in the reference [19].

DGPS sensor

The DGPS sensor measures the A/C position information based on the equations difference along the (X, Y, Z) axes. One of the important applications of the DGPS is to obtain relative position information. These sensors can

provide less than a meter scale position accuracy with nanosecond transmission accuracy. However, it should be noted, that the tanker A/Cs might overshadow the satellite vision and strongly affect the position accuracy of any satellite-based system. Considering that this type of sensor neutralizes most of the atmospheric conditions effects and system errors, a DGPS is a good solution for tracking PAD [9, 21].

MV sensor

Object recognition based on images is the subject of many studies and research. Much research is being done to improve AAR through MV sensors. The MV sensor can compare images of the tanker A/C, the relative location and rotation between the sensor and the A/C by tracking the indicator, and showing the steps for determining and estimating the situation [22, 23].

Fusion Sensor

The FS purpose is to combine the distance data provided by the MV and DGPS sensors to generate a feedback signal, as shown in Figure 3., the FS is based on the concept that when the receiver-tanker distance is greater than a certain threshold distance, only DGPS-based measurement should be used because the MV system may not be able to capture an accurate image of the drogue. As the receiver-tanker distance decreases, the target point should gradually converge towards the true drogue center. Therefore, the vector r should gradually change from the nominal position obtained by the DGPS to the position provided by the MV. Data fusion can be performed through a fuzzy fusion strategy of DGPS and MV measurements as a function of tanker-receiver distance. [23, 24].

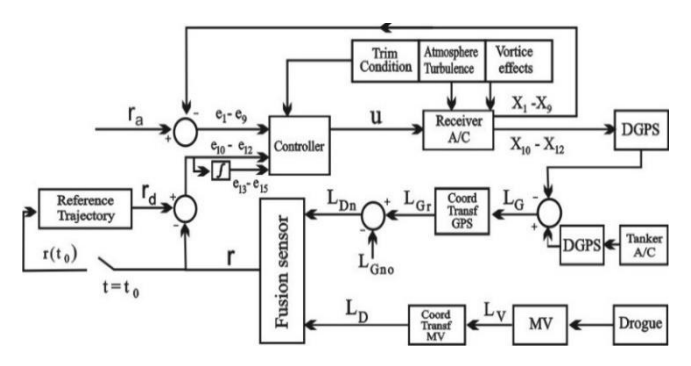


Fig. 3. The FS block diagram

The signal (r) is obtained by a FS between DGPS and MV based on the distance between two A/Cs. At large distances, the r signal is provided by the nominal DGPS distance (L_{Dn}).

$$L(t) > L_1 \text{ and } r(t) = L_{Dn}(t).$$
 (16)

In the above relation, L_1 is defined threshold distance also, in the medium distance, the r signal is obtained by combining the DGPS position and the specified MV distance:

If
$$L_2 < L(t) \le L_1 \to r(t) = \frac{1}{L_2 - L_1} \left[L_{Dn}(t) \left(d_2 - 2L_1 - L(t) \right) + L_D(t) (L(t) - L_1) \right].$$
(17)

Where
$$L_2$$
 threshold distance is defined. At a small distance, the r signal is obtained through MV. $L(t) \le L_2 \to r(t) = L_D(t)$. (18)

Eventually, from the connection stage to the end of the refueling process, the receiver and tanker A/Cs must maintain a constant relative distance equal to the value (T_d) . Because MV does not provide useful information during connection, relative position measurement is performed by DGPS (L_G) measurement. In this step, r is defined using the following equation:

$$t > T_d \rightarrow r(t) = L_G(t) - L_G(T_d). \tag{19}$$

Atmospheric turbulence

Using the Dryden turbulence model, the atmospheric turbulence effects on the hose and drogue system as well as for both the receiver and tanker A/Cs have been modeled [4]. Light turbulence is selected for AR at high altitudes and steady air.

Effects of tanker A/C

AAR is a formation flight that flies the receiver A/C in the tanker airfield. Downwash effect due to the waves produced by the tanker A/C. In AAR, since the tanker and receiver A/Cs are in a horizontal position, the downwash effects of the tanker A/C cannot be ignored. The downwash effect changes the inlet airflow angle, which changes the stability status of the A/C, resulting in the experience of various forces and momentum [25].

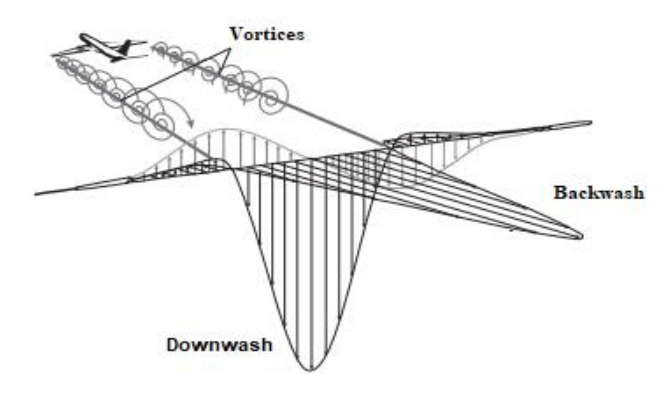


Fig. 4. Airflow disturbances from tanker A/C

Tanker A/C downwash effects

Due to the direction and pattern of the wing-tip vortices of the tanker A/C, a descending current of the air is created at the direct end of the wing.

According to Figure 4, the trailing vortices are a downward flow of air directly behind the wing. Due to this secondary effect, the surrounding air dragged around with them, which resulted in a small downward velocity component at the wing. This downward component is called downwash. The presence of downwash, and its effect on inclining the local relative wind in the downward direction, has a great effect on the airfoil AOA. This angle is given by α_{eff} and is defined as the effective AOA. According to Figure 5, the effective AOA is obtained as: $\alpha_{eff} = \alpha - \alpha_i$ where, α_i is the induced AOA and α is the geometric AOA [26].

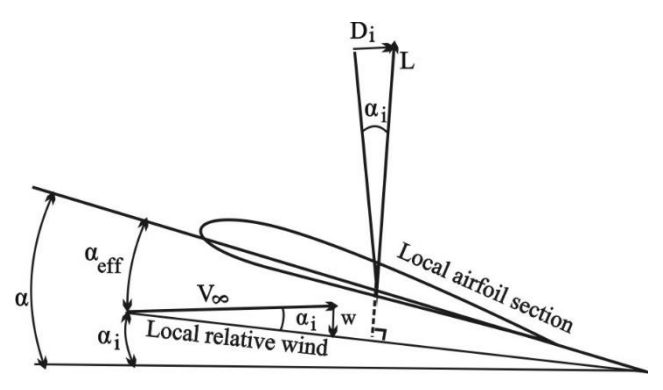


Fig. 5. The downwash effect on the AOA

Vortex effects on the receiver A/C

Since the tanker A/C flow field is not uniform, it cannot be considered a linear model. This section examines the vortex effects on the trim and control of the receiver A/C. According to Figure 6, ω_d is the downwash angle that occurs between the inbound airflow and velocity vector. Since downwash significantly affects the width of the receiver A/C, the receiver needs to be trimmed.

$$T\cos\alpha - D - mg\sin(\omega_d + \gamma) = 0.$$

$$L - mg\cos(\omega_d + \gamma) + T\sin\alpha = 0.$$

$$C_M = 0.$$

$$(20)$$

$$(21)$$

In the above equations, γ the flight path angle, L the lift, D the drag, and C_M is pitch momentum [20, 22].

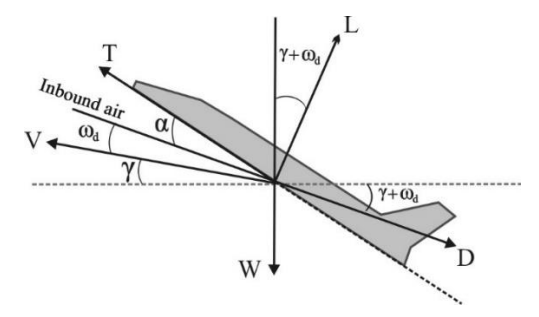


Fig. 6. The downwash effect on the lift and drag vectors direction

Trim effect

The state equations obtained in section 6.2, can be solved for X states and input values of U, which produces trim conditions. For straight and level flight:

$$\dot{X} = 0 \rightarrow \dot{u}, \dot{v}, \dot{w} = \dot{v}, \dot{\alpha}, \dot{\beta} = \dot{p}, \dot{q}, \dot{r} = 0. \tag{23}$$

After creating trim conditions, a linear dynamic model around trim flight can be obtained. This is intended as a representative that represents a nonlinear model in one area around the trim point and will be used to formulate control-based rules. State and trim input values can be obtained for flight conditions with A/C velocity and altitude.

Artificial neural networks

Artificial neural networks (ANN) based on the biological model are systems that are made up of simple, large-scale processors that have many connections between them. ANN models are trying to apply some of the rules known to the human brain. Due to its specific structure, the brain has unique features, including matching power, the ability to generalize, learning, parallel processing, error tolerance, and low energy consumption. ANNs are designed to meet some of the specifications outlined above. ANN may consists of several neurons to several thousand neurons, and the network's size depends on the problem's complexity. McCulloch and Pitts thought of modeling biological neurons for the first time in the 1940s. They developed the NN based on the mathematical model of a nerve cell. Nevertheless, in recent years, due to the ability to learn and analyze nonlinear systems, much research has been done in the field of neural networks and has been used in many scientific issues. Figure 7 shows an overview of an ANN structure. This figure shows that an ANN typically consists of three layers: 1. Input layer (as the recipient of raw data); 2. Hidden layer (as the recipient of weighting inputs), and; 3. The output layer [27-30].

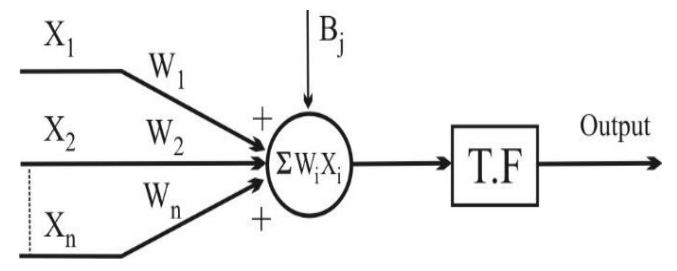


Fig. 7. The neural network structure

There are two neural network categories based on their structure, i.e., the arrangement of neurons in the model and the connections between them. Those are the feed-forward neural networks and the recurrent neural networks [31]. Feedforward neural networks are one of the simplest types of neural networks that, as their name suggests, only transmit information in one direction. This type of network consists of an input layer, an output layer, and one or two hidden layers, and the error back propagation method is used to train them. On the other hand, networks with a recurrent structure have connections that transfer information from the end layers of the network to return input. This method continues until the network reaches a stable state. This type of structure is particularly useful in problems in which the solution does not depend only on the current inputs of the system and all previous entries affect it. There are different types of feed-forward neural networks, the three most famous of which are the single-layer perceptron, the multi-layer perceptron, and the radial basis network. Similarly, recurrent neural networks are also very extensive as some of their famous networks can form a competitive network as the self-organizing mapping of Kohonen and Hopfield's network [32].

Neural networks with an ordinary sigmoid function

An ordinary sigmoid function with amplitude can be written as the following equation in which a = 1 and ρ has a constant value.

$$f(x) = \frac{a(1 - e^{-\rho x})}{(1 + e^{-\rho x})}.$$
(24)

Where a, is the function gain and ρ is the function's slope. To achieve more accuracy, the function slope and the function gain can be changed. The higher the parameters that can be adjusted, the less learning error is obtained in the neural network. Yamada's proposed design was to adjust both the slope and the gain of the sigmoid function, and he used this design in the controller [33].

Neural networks with a parametric sigmoid function

Every neural network needs a transfer function to convert input signals into output signals. Simply put, the transmission function determines the status and activation of a neuron in a neural network. In NN-PSF, the transfer function is considered a tangent hyperbolic.

$$F_q(x) = \tanh[(Lnq)x] \times (Lnq)^{-1}. \tag{25}$$

The choice of a parametric function will have three main advantages: 1. Good accuracy and high learning speed; 2. Obtaining more information about the system, and; 3. High flexibility and reducing the error range. This new form of function is desirable because it prevents the absolute function value from being underestimated due to the use of (Ln q) instead of q. The following equation can be obtained by expanding and simplifying the above equation. In this equation, the change effect of q on the sigmoid function shape can be observed [34].

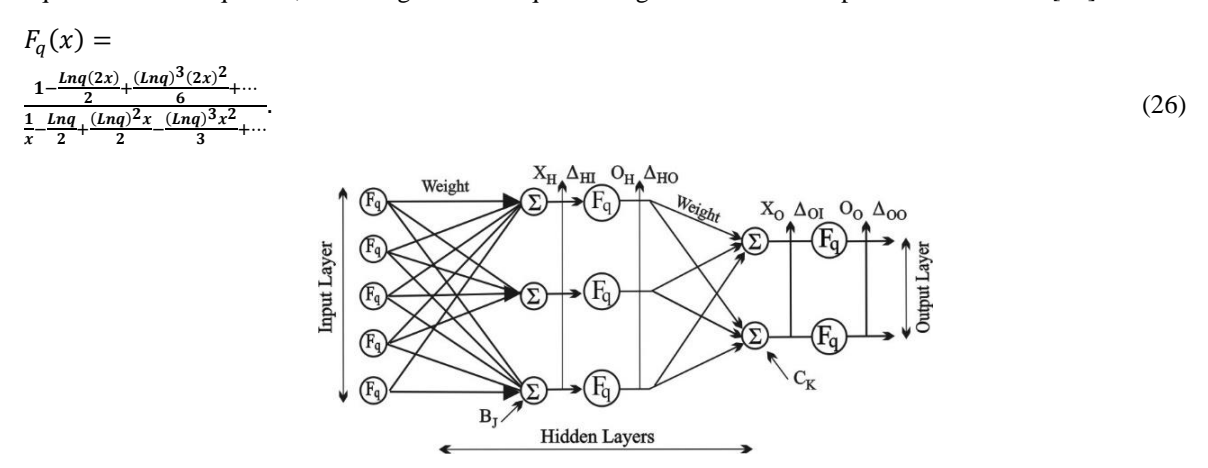


Fig. 8. The NN-PSF structure

Figure 8 shows a neural network with a parametric sigmoid function in which sigmoid functions are represented as circles. The weight coefficient is related to the output and usually equals one. The latent neuron receives the

sum of the inputs multiplied by the weight factor and produces the output. It receives the output of a k neuron and produces the output in the same state.

In this study, the neural network presented, the structured multi-layer forward network has two hidden layers. Due to the inlet and outlet variables of the receiver A/C, the input layer consists of 5 neurons, and the output layer has two neurons. The two hidden layers consist of 19 and 13 neurons, respectively. Education of ANNs is done by updating weights using backpropagation learning law. The intermediate and output layer errors are used to correct the weight coefficients. The last layer output creates an error with the desired value and the difference between them. This error is used as a weight updater. The node output is created using the multiplication node input to transfer functions concerning previous inputs. This process continues until the first layer and is eventually updated by the following equation.

$$W(t+1) = W(t) + \varphi(W(t) - W(t-1)) - \sigma h(t)$$
(27)

$$h(t) = \frac{\partial \left(\sum_{j=1}^{N} (d_j - p_j)\right)}{\partial w_{ji}}.$$
 (28)

$$Error = \frac{1}{2} \sum_{k} (d(k) - o(k))^{2}.$$
 (29)

Where d (k) is the desired output value for kth output.

In the learning phase, error signals propagate backward through the network. The q-parameter is adjusted by tuning the weighting coefficients to minimize the error between the network output and the training and learning signals.

Effect of "q" parameters (NN-PSF learning)

In this paper, the transfer function used a tangent hyperbolic. Since the parameter "q" defined in the transfer function causes it to adapt, it plays an important role in PNN. Changes in this parameter proportional to the nonlinear degree, and changes in the data set help the network learning process. The standard form of hyperbolic function is equation 25. The control of this function is performed by parameters a, ρ (equation 24). To prevent severe changes in these parameters, instead of "a" the limiting function $\frac{1}{\ln q}$ or e^{-q} are used. The "q" parameter has the regulator role for the transfer function. Finally, the effect of the "q" parameter changes in the following equations are shown.

$$q_{new} = q_{old} - \rho \frac{\partial E}{\partial q_{old}}. (30)$$

Where ρ is the learning rate.

$$\Delta_{oo}(k) \triangleq \frac{\partial E}{\partial o_o(k)} = o_o(k) - d(k). \tag{31}$$

$$\Delta_{oi}(k) \triangleq \frac{\partial E}{\partial x_0(k)} = \frac{\partial E}{\partial o_o(k)} \frac{\partial o_o(k)}{\partial x_0(k)} = \Delta_{oo}(k) \times \tanh'(\ln q_k \times x_0(k)). \tag{32}$$

$$\Delta_{ho}(j) \triangleq \frac{\partial E}{\partial o_h(j)} = \sum_k \frac{\partial E}{\partial x_0(k)} \frac{\partial x_0(k)}{\partial x_h(j)} = \sum_k \Delta_{oi} \times$$

(33)

$$\Delta_{hi}(j) \triangleq \frac{\partial E}{\partial_{xh}(j)} = \frac{\partial E}{\partial_{oh}(j)} \frac{\partial_{oh}(j)}{\partial_{xh}(j)} = \Delta_{ho}(j) \times tanh' \left(\ln q_j \times x_h(j) \right). \tag{34}$$

For q in the k^{th} output neuron.

$$\begin{split} \frac{\partial E}{\partial q_k} &= \frac{\partial E}{\partial o_o(k)} \frac{\partial o_o}{\partial q_k} = \frac{-1}{q_k \times \ln q_k} \times \{\Delta_{oo}(k) \times o_o(k) - \Delta_{oi}(k) \times x_0(k)\}. \end{split} \tag{35}$$

For q in the hidden neuron, the gradients can be calculated as,

$$\frac{\partial E}{\partial q_j} = -\frac{1}{q_j \times \ln q_j} \times \{ \Delta_{ho}(j) \times o_h(j) - \Delta_{hi}(j) \times x_h(j) \}. \tag{36}$$

All the weights and "q" parameters can be updated using the above error signals [29, 33].

Parametric neural networks training

After selecting the type of NN, it is time to train them. It has two data groups. A data group is an input vector to the network, which includes control variables and A/C states at different moments. The second data group is the desired output of each network at any moment. In other words, it is the amount that is expected to produce a specific input for a vector [14]. Figure 9 shows the parametric neural network training.

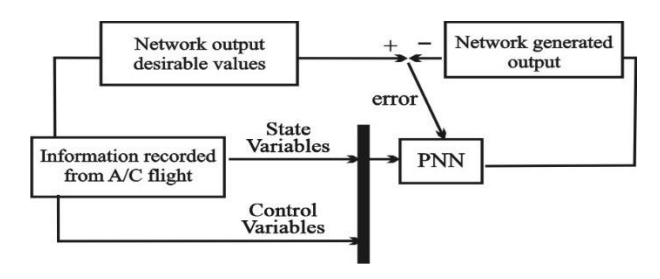


Fig. 9. The network training method schematic

Neural network training is done with the available data. In practical work, the data is obtained through flight testing [15]. In this study, the analytical simulation output was used for training due to a lack of flight test data. This means that the simulated models are applied to a receiver A/C, and the results are recorded for use in the training process. It is noteworthy that the identification method presented in this study can be applied to the test results extracted from the actual flight test. In other words, if the model works properly for simulator outputs, this method can also be applied to flight test data.

System identification

System identification is the process of appropriate use of mathematical models and learning algorithms to draw a map of experimental data by minimizing an error criterion between the desired system output and the model output. The autoregressive moving average (ARMA) model are linear regression model which is presented below in discrete form [36]

$$y(k) = a_0 x(k) + \dots + a_n x(k-n) + b_1 y(k-1) + \dots + b_m y(k-1)$$
m). (37)

Where x(k) and y(k) are the model's input and output. Another way to show is as follows:

$$y(k) = \sum_{i=0}^{n} a_i x(k-i) + \sum_{j=1}^{m} b_j y(k-j).$$
 (38)

Where a_i and b_i are the model's parameters at sample k. The transfer function is obtained as follows:

$$T.F = H(z)$$

$$= \frac{a_0 + a_1 z^{-1} + \dots + a_n z^{-n}}{1 - b_1 z^{-1} - \dots - b_m z^{-m}}.$$
(39)

Equation 37 can be contracted as a vector format $y(k) = \alpha^T \beta(k)$ where $\alpha^T = [b_1, ..., b_m, a_0, ..., a_n]$ is the parameter vector and $\beta(k) = [y(k-1), ..., y(k-m), x(k), ..., x(k-n)]^T$ is the measurement vector. The block diagram of general system identification is shown in figure 10.

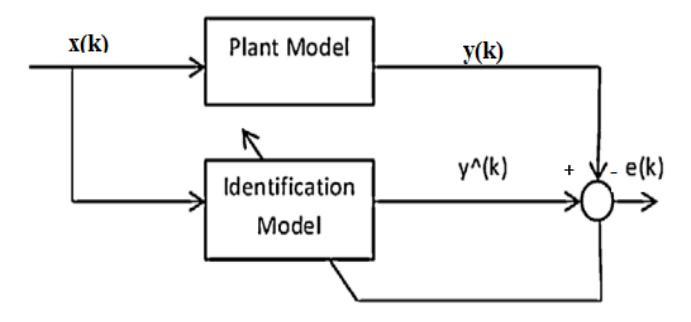


Fig. 10. Block diagram of general system identification

Algorithms such as least squares (LS), recursive least squares (RLS), and recursive prediction error method (RPEM) are used for system identification purposes. [35, 36]. Since most existing physical systems are nonlinear, therefore they require nonlinear modeling. However, the existence of nonlinear relationships between the input and output of dynamic systems, makes it difficult to identify different types of these systems with accurate parametric models. Identification of such models should be done through the Volterra series and the Hammerstein model. To modify the linear ARMA model and create a nonlinear ARMA model there would be

$$y(k) = \sum_{i=0}^{n} a_i \ x(k-i) + \sum_{j=1}^{m} b_j \ y(k-j) + \sum_{i=0}^{n} \sum_{j=0}^{m} a_{ij} \ x(k-i)x(k-j) + \sum_{i=1}^{n} \sum_{j=1}^{m} b_{ij}y(k-i) y(k-j) + \sum_{i=0}^{n} \sum_{j=1}^{m} c_{ij} x(k-i) y(k-j) + \sum_{i=0}^{n} \sum_{j=1}^{n} c_{ij} x(k-i) y(k-j) + \sum_{i=0}^{$$

In the nonlinear form of ARMA, New parameters ((a_{ij} , b_{ij} , c_{ij}) are added [37].

PNN identification (reference path)

The reference path built to link the probe and the drogue must meet these two crucial criteria: To prevent a collision between the two A/Cs and the drogue hose system, one must first ensure the safety of both A/Cs and the refueling accessories. Additionally, the drogue movement, while affected by current disturbances, shouldn't necessarily disrupt the path's overall design. As a result, the vertical position error between the probe and the drogue in the first portion of the path has been fixed, and now the drogue's movement in the last part of the route has to be taken into account. Furthermore, the planned route needs to work while considering the receiver A/C's dynamic restrictions. A consistent and obvious, smooth path needs to be created to satisfy the second criterion. Figure 11 depicts the reference path layout between the two A/Cs (receiver and tanker).

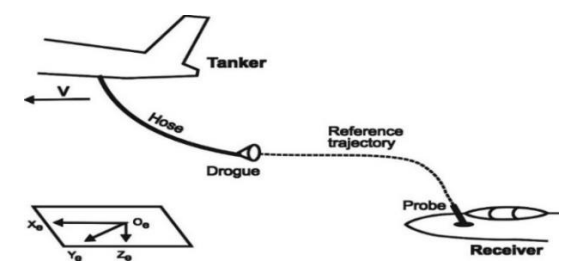


Fig. 11. Structure of the reference path

Now to create the reference path, when the AR process between the two A/Cs begins at the time t_0 . The receiver A/C control rules must create a suitable route to achieve the desired r_s target at a reasonable time despite the receiver A/C dynamic constraints. Therefore, this method is defined to program a smooth reference path r_d that is avoided by following the distance r from high accelerations and velocities. In designing the reference path, the speed and height are assumed to be constant.

$$r_{\alpha} = [V, \alpha, \beta, P, q, r, \phi, \theta, \Psi]_{ref}^{T} = [V_{n}, \alpha_{n}, \beta_{n}, 0, 0, 0, 0, \theta_{n}, \Psi_{n}]^{T}.$$

$$(41)$$

Where the index n shows the connection point values. The position and interpolation of the cube are used to form the reference path components $r_d = \left[r_{dx}, r_{dy}, r_{dz}\right]^T$. That means:

$$r_{di}(t) = a_i t^3 + b_i t^2 + c_i t + di, \ i = x, y, z.$$
(42)

Where the coefficients a_i , b_i , c_i and d_i are obtained through the following boundary conditions. By setting the initial maneuver time at $t_0 = 0$ and keeping the optimal final maneuver time constant at $t_{di} = T_{di}$, it is necessary to:

$$r_d(t_0) = r_i(0)$$
, $r_{di}(T_{di}) = 0$, $i = x$, y , z . (43)

In addition, the initial and final speeds of the reference signals are considered to be zero:

$$\dot{\mathbf{r}}_{di}(0) = 0, \ \dot{\mathbf{r}}_{di}(T_{di}) = 0, \ i = x, y, z.$$
 (44)

Algebraic calculations show that Equation 42 solves constraints 43 and 44 with the following equations.

The maximum velocity and acceleration values along the path are obtained as follows.

$$r_{di}(t) = \frac{2r_{i}(0)}{T_{di}^{3}} t^{3} - \frac{3r_{i}(0)}{T_{di}^{2}} t^{2} + r_{i}(0)$$

$$0 \le t \le T_{di} \quad i = x, y, z. \tag{45}$$

The maximum speed and acceleration values along the path are obtained as follows:

$$V_{\text{max }i} = -\frac{3r_i}{2T_{di}}$$
. $AC_{\text{max }i} = \pm \frac{6r_i(0)}{T_{di}^2}$. (46)

The initial position distance vector $[r_{dx}(0), r_{dy}(0), r_{dz}(0)]$ in the above equations can be used to obtain the minimum maneuver time T_{di} ; which guarantees the desired values for maximum speed or acceleration. In this paper, the receiver A/C direction along the Y-Z plane of the ORRF frame and then the direction along the X direction for maneuvering is selected. The connection sequence is longer than the other two, given the maneuvering time (T_{dx}) along the forward X direction. Based on this we will have [19, 38].

$$T_{yz} = \max(T_{dy}, T_{dz}) \to If \left(T_{dx} < T_{yz}\right) \xrightarrow{then} T_{dx} = T_{yz} + 5 s. \tag{47}$$

III.SIMULATION AND DISCUSSION

A MATLAB-based simulation environment has been developed to simulate the AAR docking stage. It should be noted that in NNs with PSF, due to the use of additional parameters in the performance function, it has more power in the detection, identification, and flexibility of the AR system. In the docking phases, training errors will normally decrease during the initial training phase. If tracking error is increased between the drogue (tanker A/C) and probe (receiver A/C), the weights have to be adjusted the process goes back to evaluate the output of the network. The weights of the connections will then be adjusted to get the network output closer to the desired state. Repeating this technique results in good convergence and a decreased error value. The inaccuracy in the training phase, however, tends to rise as the PNN attempts to match the data. The training terminates and the weights and bias return to the level with the least amount of error once the tracking error has grown for a certain number of iterations. In NN-PSF networks, there is at least one reversal signal from one neuron to the same neuron or neurons of the same layer or previous layers. Reversible networks can show behavior related to the temporal properties and dynamics of systems. In this type of network, which is designed according to the dynamic nature of the

problem, after the network learning stage, the parameters are also changed and corrected. In this paper, state variables are the relative position coordinates of the PAD (x, y, z), velocities (u, v, w), angular velocities (p, q, r) and altitude angles (ϕ , θ , Ψ) under the body coordinate system of receiver A/C. The control (input) variables are selected δ_a , δ_e , δ_r , δ_t . The output variables are the relative position coordinates of the probe to the drogue under the ground coordinate system of receiver A/C. The following data have been used for numerical simulation and modeling [39].

$$\text{M=8.838} \times 10^5 \text{kg}, \ \overline{c} = 8.763 \ m \ \text{b=39.877} \ \text{m}, \ \ I_{xx} = 3.186 \times 10^4 kg.m^2, \ I_{yy} = 8.757 \times 10^4 kg.m^2, \ I_{zz} = 1.223 \times 10^5 kg.m^2 \ I_{xz} = -546.394.kg.m^2 \ \text{S} = 226.03m^2$$

$$C_{D\delta e^2}=0.25,~C_{s0}=0,~C_{D0}=0.023,~C_{D\alpha}=0$$
 , $C_{D\alpha^2}=0.7,~C_{D\delta e}=0~C_{s\beta}=-0.812,~C_{s\delta r}=0.184,~C_{L0}=0.1$

$$\begin{array}{l} C_{L\alpha}=4.8, \quad C_{L\alpha^2}=0, \quad C_{Lq}=5.65, \quad C_{L\delta r}=0.19, \quad C_{l0}=0, \quad C_{l\delta a}=-0.05, \quad C_{l\delta r}=0.019, \quad C_{l\beta}=-0.177, \quad C_{lp}=-0.312, \quad C_{lr}=0.1153, \quad C_{l\delta e}=0, \quad C_{M0}=0, \quad C_{Mq}=4.5, \quad C_{M\alpha}=-0.65, \quad C_{M\delta e}=-0.57, \quad C_{N0}=0, \quad C_{N\delta a}=0.008, \quad C_{N\delta r}=-0.076, \quad C_{N\beta}=0.129, \quad C_{Np}=-0.011 \quad and \quad C_{Nr}=-0.165 \quad x(0)=130m \,, \\ y(0)=25m, \quad z(0)=30m, \quad V(0)=180\frac{m}{s}, \quad \alpha(0)=0.03 \, rad, \quad \theta(0)=0.02 \, rad, \quad \gamma(0)=0 \, rad, \\ q(0)=0\, \frac{rad}{s} \quad {}_{3}L_{G}(0)=[130,25,30]m \, {}_{3}L_{Gno}(0)=[20,0,10]m \, {}_{3} \quad r_{d}=[6,0,0]m, \quad L_{D}(0)=[130-20,\ 25-0\ ,30-10]=[110,25,20] \end{array}$$

In this regard, to obtain the convergence of the network output and the real output, after modeling the receiving A/C and obtaining the input and output through MATLAB software, the following results were obtained:

Figure 12 (a) shows tracking error value vs. iteration and (b) shows the convergence of network output and real output in the X direction. As can be seen, the amount of tracking error is close to 0.0001 after 2000 iterations and also, the convergence of the network output with the real output is obtained.

Figure 13 (a) shows the tracking error value vs. iteration and (b) shows the convergence of network output and real output in the Y direction. As can be seen, the tracking error amount is close to 0.001 after 10000 iterations, and also, the convergence of the network output with the real output is obtained.

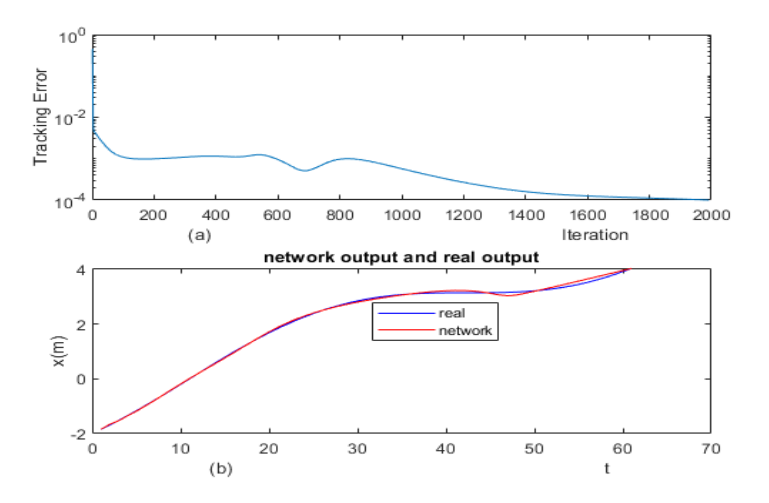


Fig. 12. (a) Tracking error value vs. iteration (b) Convergence of network output and real output in the X direction

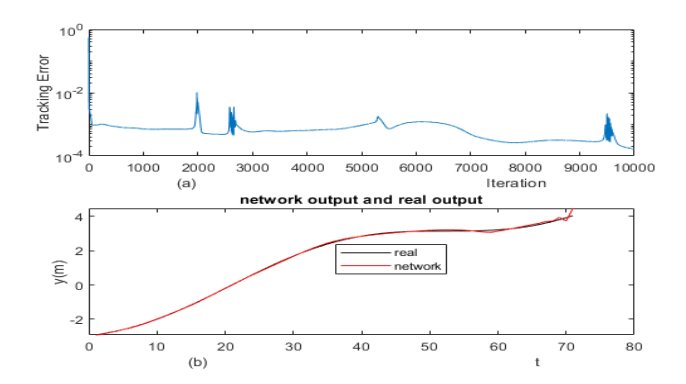


Fig. 13. (a) Tracking error value vs. iteration (b) Convergence of network output and real output in Y direction

Figure 14(a) shows tracking error value vs. iteration and (b) shows the convergence of network output and real output in the Z -direction. As can be seen, the tracking error amount is close to 0.0001 after 2500 iterations, and also, the convergence of the network output with the real output is obtained.

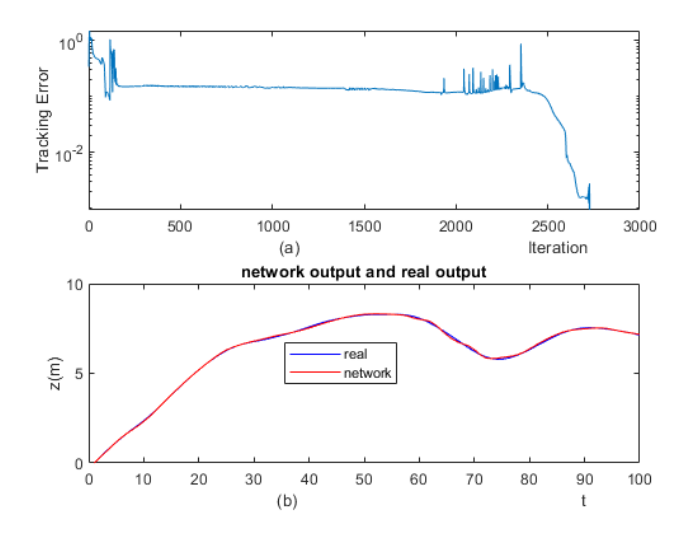


Fig. 14. (a) Tracking error value vs. iteration (b) Convergence of network output and real output in the Z direction

Figure 15 shows the drogue and the probe trajectory. Due to the non-uniform turbulence of the tanker A/C, the hose and drogue system gradually stabilize at equilibrium. The drogue position around the equilibrium will also fluctuate due to turbulence.

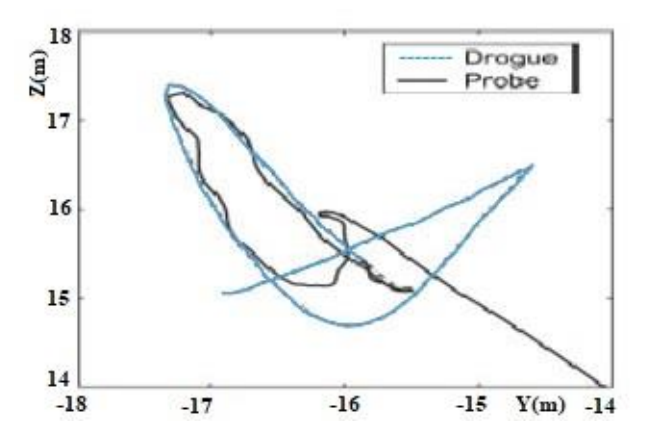


Fig. 15. Drogue and probe trajectory

The results of tracking the position of the receiver A/C, taking into account the effects of the tanker A/C, are extracted as follows:

Figure 16, results comparison of the position tracking of the receiver A/C considering the tanker A/C effects.

Figure 17 shows the drogue displacement with stable flight conditions. As can be seen from the figure, after 90 seconds, the drogue oscillations due to turbulence in the three directions X, Y and Z, converge to stable conditions.

The elements of the r signal and the matching reference that creates the programmed path are shown in Figure 18. With the connecting maneuver, 90 seconds is the ideal tracking period for the three components. With the help of the NN-PSF rule, the receiver A/C can precisely monitor the drogue. The connection stages are pretty successful in 90 seconds because detection faults satisfy the requirements of the connection step.

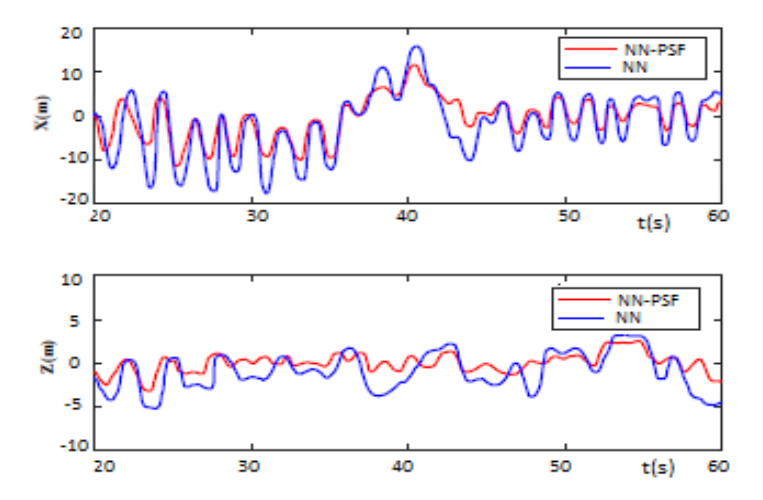


Fig. 16. Position tracking of the receiver considering the tanker effects in two directions of X and Z

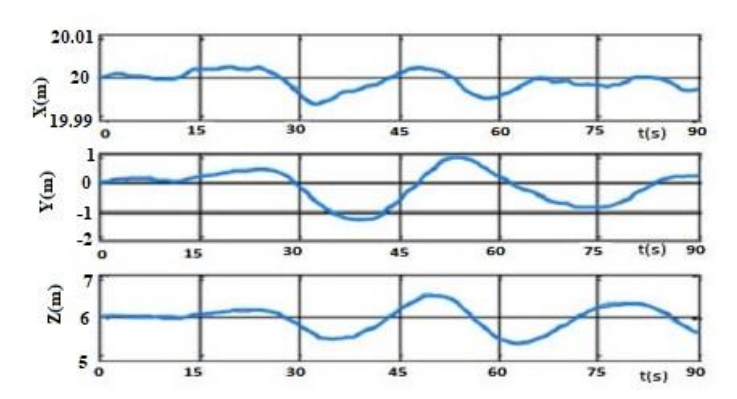


Fig17. Drogue displacement vs time in three direction X, Y, Z

Figure 19 shows the time response of system states, including velocity, path angle, turn angle, and turn angle rate. As shown in Figure 19, by simulating MATLAB software, the speed and angle of the path converge to the nominal conditions. The pitch angle and rate change rapidly to compensate for external turbulence effects.

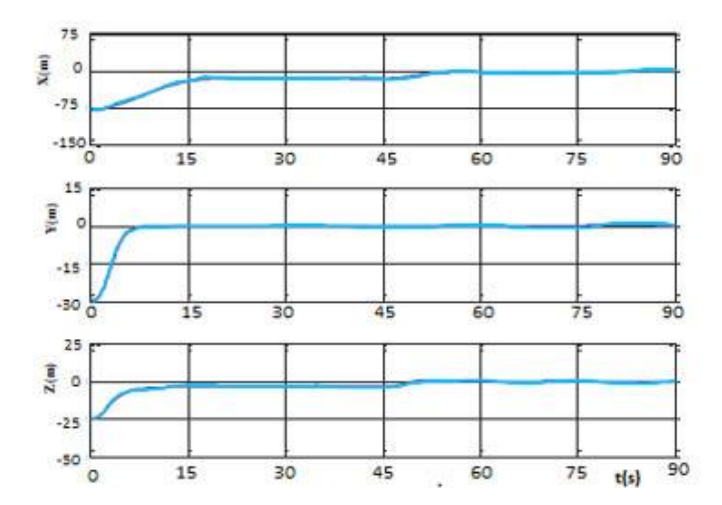


Fig. 18. Path tracking error during the connection phase in three directions X, Y, Z

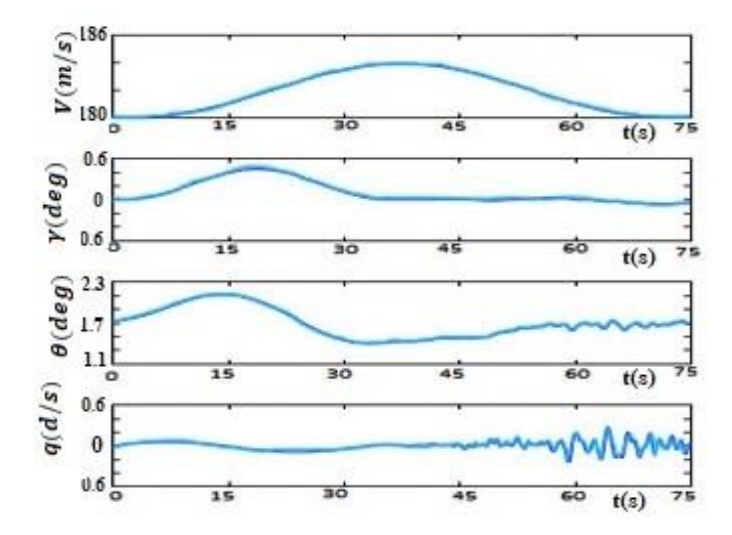


Fig. 19. Time response of receiver A/C modes

Figure 20 shows the steps before and after the refueling connection in three directions. As it is known, before connection, the drogue will fluctuate a lot due to the non-uniform waves of the tanker A/C. However, from the moment the two A/Cs connect, they gradually reach a steady state of equilibrium.

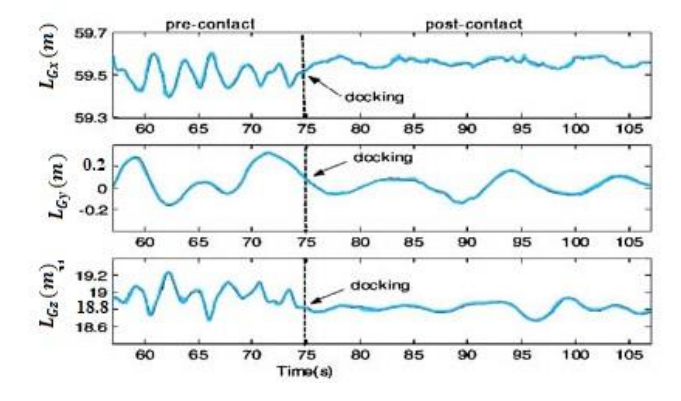


Fig. 20. L_G vector components during the AR process

IV.CONCLUSION

This research studies the AR system mechanism model in the presence of disturbance effects and proposes a method based on neural network with parametric sigmoid function for air refueling detection. After determining

the mathematical model, the input and output values of the modes were extracted using MATLAB software. The final analysis and conclusion of this research can be summarized as follows:

- 1. In this research, the NN-PSF method was used to identify A/C in order to use its results in the development of AAR. In the proposed method, which provides advantages such as the ability to learn and the ability to adapt to new conditions, such as the lack of comprehensive information about the structure of the nonlinear model in the presence of disturbances, the graphs are continuously estimated.
- 2. In the proposed method, three different forms of neural network including normal sigmoid function, parametric sigmoid function and parametric sigmoid function with natural logarithm are used to identify the air refueling system. By implementing all of them and comparing the results, it was found that the neural network with the parametric sigmoid function method (natural logarithm) has three main advantages over others: 1. Greater reduction of the error between the receiver and the tanker, 2. Obtaining limited and uniform signals, and; 3. The ability to learn the system in turbulent aerodynamic conditions and uncertainty.

The following can be considered for the future development of this research:

- Compared to reality, there are certain differences in modeling and identification for future research. For example, applying a sudden and momentary load causes elasticity and wear of the probe and drogue.
- To ensure the correctness of the proposed model, possible simulated results will be compared with real data in future research, as practical confirmation is possible by conducting refueling flight tests.

REFERENCES

- [1] Joint Air Power Competence Center. ATP-3.3.4.10, "Automated Air-to-Air Refueling (A3R)," Allied Tactical Publication, Ed.; NATO Standardization Office (NSO), Brussels, Belgium, 2021.
- [2] Vergun, D, "AR adds Lethality to DOD Aviation," DOD news, Feb. 21, 2020.
- [3] F. Morscheck, and M.Li, "Benefits and challenges of a civil air to air refuelling network analysed in a traffic simulation," IEEE/AIAA, 34th Digital Avionics Systems Conference, Prague, Czech republic, 2015.
- [4] P.R.Thomas, U.Bhandari, S. Bullock, T.S. Richarson, and J.L.D. Bois, "Advances in air to air refueling," Progress in Aerospace sciences 71, pp14-35, 2014.
- [5] Christopher, B., and J. D, K., "Air Force AR Methods: Flying Boom versus Hose-and-Drogue," Digital Library, Retrieved 27 October 2017.
- [6] Jiang feng, CH., and Kang, J., "Dynamic modeling and simulation of variable –length hose drogue AR systems," AIP Advances 12, 015104, 2022. AIP Advances 12, 015104 (2022)
- [7] M.K. Filyashkin, "Approach of a tanker A/C to the remote-controlled drogue of air to air refueling system," IEEE 4th international conference UAV, kiev Ukraine, 2017.
- [8] Shi, B., Liu, Z., and Zhang, G., "Vision Sensor for Measuring Aerial Refueling Drogue Using Robust Method," IEEE sensors Journal, 21, PP. 28037–28049, 2021.ieeexplore.ieee.org
- [9] Parry, J., and Hubbard, S., "Review of Sensor Technology to Support Automated Air-to-Air Refueling of a Probe Configured Un crewed A/C," Sensors, 23(2), 995, 2023.
- [10]G.Campa, M.R.Napolitano, and M.L.Fravolini, "Simulation Environment for Machine Vision Based Aerial Refueling for UAVs," IEEE Trans, Aeros. Election. Syst, vol. 45, no. 1, pp. 138-151, Jan IEEE Log No, 2009.
- [11] Nakpil, and M.R. Ananthasayanam, "Relative position and attitude estimation and control schemes for the final phase of an autonomous docking mission of spacecraft," ActaAstronauticapp.511-522, 2009.
- [12] B. Sinopoli, M. Micheli, M. Donato, and T.J. Koo, "Vision based navigation for an unmanned aerial vehicle," Proceedings of the IEEE International Conference on Robotics and Automation, Seoul, South Korea, pp.1757-1764, 2012.
- [13] L. Borui, M. Chundi., and W. Botao, "A Survey of vision based autonomous AR for unmanned aerial vehicles," IEEE, International Conference on Intelligent Control and Information Processing, pp 207-213, 2017.
- [14] L.R. Mash, "Toward automated AR: automated visual A/C identification with convolutional neural networks" PHD thesis, Wright-Patterson Air Force Base, Ohio, 2017.
- [15] L.R.Mash, B.Borghetti, and J.Pecarina, "Improved A/C recognition for AR through data augmentation in convolutional neural networks," proceedings of the 2012th international symposium on visual computing, 2016.
- [16] H.Keyhanifar, R.Zardashti, J.Pirkandi, and K. Malekzadehfard, "Control design of an AR system using a combination of machine vision and GPS taking into account the vortex flow effects of the refueling A/C," Scientific Journal of Aviation Engineering, pp. 167-185,2022.
- [17] A. Kanazawa, A. Sharma, and D. Jacobs, "Locally Scale-invariant Convolutional Neural Network," Deep Learning and Representation Learning Workshop: Neural Information Processing Systems Conference, pp. 1–11, 2014.

- [18] A. Krogh, and J. Vedels by, "Neural Network Ensembles, Cross Validation, and Active Learning," Advances in Neural Information Processing Systems, pp. 231 238, 1995.
- [19] M.L. Fravolini, A.Ficlo, G.Campa, M.R.Napolitano, and B. Seanor, "Modeling and control issues for autonomous AR for UAV using a probe drogue refueling system," Aerospace science and technology, pp. 611-618.2004.
- [20] Y. Liu, H. Wang, and J. Fan, "Novel docking controller for Autonomous AR With probe direct control and learning based preview method," Aerospace science and Technology, pp. 1-14, 2019.
- [21] Krasuski, K., Popielarczyk, D., Cie, A., and C. wiklak, J., "A New Strategy for Improving the Accuracy of A/C Positioning Using DGPS Technique in Aerial Navigation," Energies 14(15), 4431, 2021.
- [22] M. Mammarella, G. Campa, M.R. Napolitano, M.L. Fravolini, Y. Gu, and M.G. Perhinschi, "Machine Vision/GPS Integration using EKF for the UAV AR problem," IEEE Transactions systems, man and cybernetics- part c applications and reviews, vol. 38, No. 6,2008.
- [23] M.L. Fravolini, A. Ficlo, G. Campa, M.R.Napolitano, B. Seanor, and M.G. Perhinschi, "Autonomous AR for UAVs using a combined GPS-Machine vision guidance," AIAA Guidance, Navigation, and control conference and exhibit 16-19, Rhode Island.2004
- [24] Peng, J.; Zhang, P.; Zheng, L.; Tan, J. UAV Positioning Based on Multi-Sensor Fusion. IEEE Access 2020, 8, 34455–3446
- [25] S.C. Kriel, J.A. Engelbrecht, and T. Jones, "Receptacle normal position control for automated aerial refueling," Aerospace Sci, Technol. pp. 296-304. 2013
- [26] J. D. Anderson, "Fundamental of aerodynamics" Curator of Aerodynamics National Air and Space Museum Smithsonian Institution and Professor Emeritus University of Maryland, Third Edition.
- [27] Aggarwal, C.C., "An Introduction to Neural Networks" Neural Networks and deep learning, PP 1-52, 2018.
- [28] Bommana, H., "Introduction to Neural Networks Part 1," Deep Learning Demystified, 2019.
- [29] K. Gurney, "An introduction to neural networks," university of Sheffield London and New York, published in the Taylor & Francis e-Library, 2004.
- [30] W.S. McCulloch, and W. Pitts, "A Logical Calculus of Ideas Immanent in Nervous Activity," Bulletin of Mathematical Biophysics, pp.127-147,1943.
- [31] S. Hykin, "Neural networks: A comprehensive Foundation", 2nd ed, Prentice-Hall, 1999.
- [32] A. Jain, J. Mao, and K.M. Mohiuddin, "Artificial Neural Networks: A Tutorial," IEEE Computer Soc. Press, Vol. 29, Issue 3, pp. 31-44, 1996.
- [33] T. Yamada, and T. Yabuta, "Neural network Controller using autotuning method for nonlinear Functions," Trans, on NN-3-4, pp.595-601, 1992.
- [34] M. Hasheminejad, J. Murata, K. Hirasawa, and S. Sagara, "System Identification Using Neural Networks with parametric Sigmoid Functions," Trans. Soc. Instrument, Control Eng. pp.277–283, 1995.
- [35] R. Isermann, M. Munchhof, Identification of Dynamic Systems: An Introduction with Applications, Springer, 2011.
- [36] T.S. Soderstrom, P.G. Stoica, System Identification, Prentice Hall, 1989.
- [37] T.A. Tutunji, Parametric system identification using neural networks, Applied Soft Computing 47 (2016) 251–261.
- [38] H. Zhu, S. Yuan, and Q. Shen, "Vision/GPS-based docking control for the UAV autonomous aerial refueling," IEEE, Conference, pp. 1211-1215, 2016.
- [39] Napolitano, M.R., "A/C Dynamics: From Modeling to Simulation," Department of Mechanical and Aerospace Engineering Flight Control Research laboratory, Director West Virginia University, PP 11-720, 201